Energy Storage Structural Composites: a Review

TONY PEREIRA[1,*], ZHANHU GUO[1], S. NIEH[2], J. ARIAS[2] AND H. THOMAS HAHN[1,3]

[1]*Mechanical and Aerospace Engineering Department, University of California Los Angeles, CA 90095, USA*

[2]*Front Edge Technologies, Inc., Baldwin Park, CA, USA*

[3]*Materials Science and Engineering Department, University of California Los Angeles, CA 90095, USA*

ABSTRACT: This study demonstrates the construction of a multifunctional composite structure capable of energy storage in addition to load bearing. These structures were assembled and integrated within the confines of a multifunctional structural composite in order to save weight and space. Carbon fiber reinforced plastic (CFRP) composites were laminated with energy storage all-solid-state thin-film lithium cells. The processes of physically embedding all-solid-state thin-film lithium energy cells into carbon fiber reinforced plastics (CFRPs) and the approaches used are reviewed. The effects of uniaxial tensile loading on the embedded structure are investigated. The mechanical, electrical, and physical aspects of energy harvesting and storage devices incorporated into composite structures are discussed. Embedding all-solid-state thin-film lithium energy cells into CFRPs did not significantly alter the CFRP mechanical properties (yield strength and Young's modulus). The CFRP embedded energy cells performed at baseline charge/discharge levels up to a loading of about 50% of the ultimate CFRP uniaxial tensile rupture loading.

KEY WORDS: multifunctional composites, all-solid-state thin-film lithium battery, embedding, energy storage.

INTRODUCTION

THE PHYSICAL PROPERTIES of thin-films of a few hundred nanometers to tens of micrometers in thickness are radically different from those found in the bulk material [1]. Exploring applications for these new thin-film devices has opened a new frontier in engineering and materials science with resulting configurations that can combine thermoelectric, piezoelectric, photovoltaic, energy storage, sensors, actuators and controls in a multifunctional composite laminated structure (Figure 1). The main objectives of this study were to successfully embed all-solid-state thin-film lithium energy

*Author to whom correspondence should be addressed. E-mail: apereira@ucla.edu

Figures 1–3 and 5–13 appear in color online: http://jcm.sagepub.com

0021-9983/09/05 0549–12 $10.00/0 DOI: 10.1177/0021998308097682

cells into CFRPs, resulting in composite laminated structures with energy storage capability. Successful embedding means that the embedded energy cell would still be able to charge and discharge at levels within its baseline parameters obtained prior to the embedding process. This process was carried out in three consecutive steps: investigate the ability of the energy cells to withstand flexure, then uniaxial pressure and finally, autoclave curing. Our approach was to use all-solid-state thin-film lithium energy cells directly embedded in composite laminates, to develop methods of structural integration and to evaluate both structural and energy storage performances. The performance of thin-film batteries under deformation and pressure is not well understood, and the effect of the manufacturing environment on battery performance is not known. The benefits of this investigation are to create enabling technology to reduce weight and space for many DoD systems (Figure 2).

Hybrid laminated composites can now be made by embedding micro-thin-film energy-storage, piezoelectric, photovoltaic and thermoelectric devices into the structure of composite laminates with multifunctional capabilities specifically designed to fit conformal spaces and envelopes, and engineered to save weight and space. The properties of each can be fine tuned to meet special requirements. Particular care and consideration is required

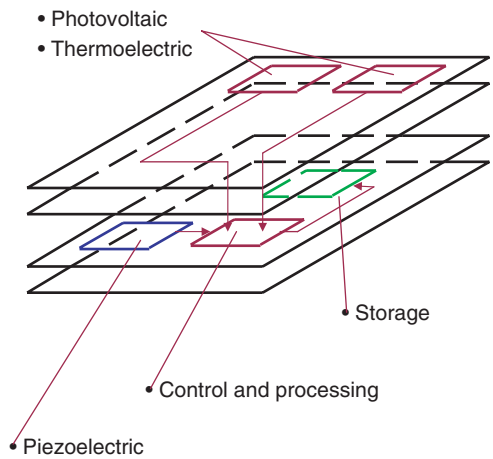

Figure 1. *Energy harvesting multifunctional structures integrating thermoelectric, piezoelectric, photovoltaic and energy storage elements.*

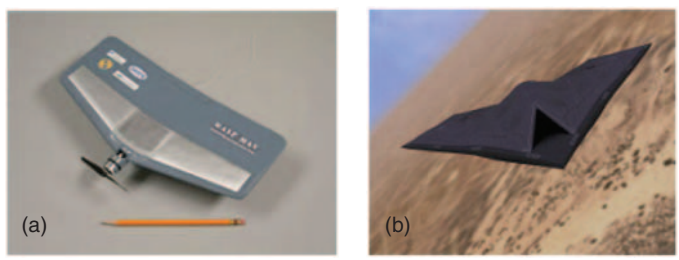

Figure 2. *Unmanned aerial vehicles are designed in a wide range of sizes and shapes to fit multiple missions: (a) Wasp from AeroVironment, (b) Taranis from BAE-Systems.*

for the manufacture of these assemblies due to the wide range of physical characteristics of its components. In this process, supplementary functionality and capabilities are added optimally to the volumetric space traditionally used only for simple mechanical and structural reinforcement, i.e., the conformal space dedicated to the absorption of stress, strain and mechanical energy.

An additional advantage of the final structure hence obtained is that, due to the fact that the thin-film devices and their substrates become embedded into the CFPRs, the thin-film devices also benefit from this integration and become thus significantly more resilient to deterioration or damage from external physical forces or agents than what the thin-film devices and their substrates are able to withstand if deployed into the physical environment all by themselves. The capabilities added to the integral composite structure of the assembly encasement and to the overall structural component and structural envelope provide additional functionality to the desired mechanical and physical properties required for the structural integrity of the whole. Furthermore, the mechanical properties of the structural element can be fine tuned to fit optimally the stresses encountered in the operational environment.

Multiple applications for this technology can be found as multifunctional materials to supply power for micro-pumps, Lab-on-a-Chip, micro-actuators, medical implants, mobile equipment, drug delivery systems, autonomous remote sensing, integrated energy harvesting and storage devices [2], personal digital assistants (PDAs), smart structures and controls, active radio-frequency identification (RFID), health monitoring systems (HMS), portable personal computers, micro-satellites [2,3], micro-electromechanical systems (MEMS) for satellites, autonomous micromechanical sensors and actuators [4], MEMS and bio-MEMS [5], micro aerial vehicles (MAVs) [6], unmanned aerial vehicles (UAVs, see Figure 2) [7] and where autonomous electrical power is required without the extra weight and difficulty of running hook up electrical service wires.

EXPERIMENTAL

Front Edge Technologies (Baldwin Park, CA) provided the all-solid-state thin-film lithium energy cells (Figure 3). These energy cells are currently in commercial production, with a nominal voltage of 3.6 VDC [11], a lifetime of 1000 charge/discharge cycles of up to 100% depth-of-discharge and a specific energy of about 200 Wh/kg without considering the packaging mass. The energy cell packaging for the configuration used in this study

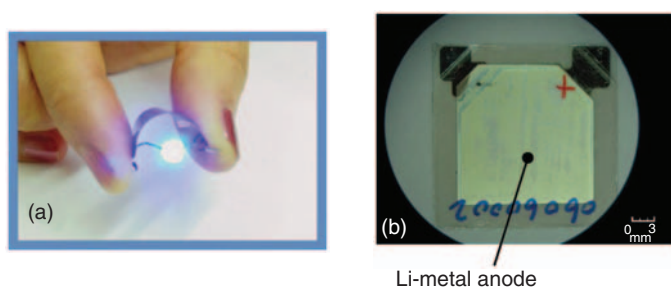

Figure 3. *All-solid-state thin-film lithium energy cells from Front Edge Technologies: (a) flexed, powering a blue LED; (b) the type used in this work, lithium-metal anode facing up.*

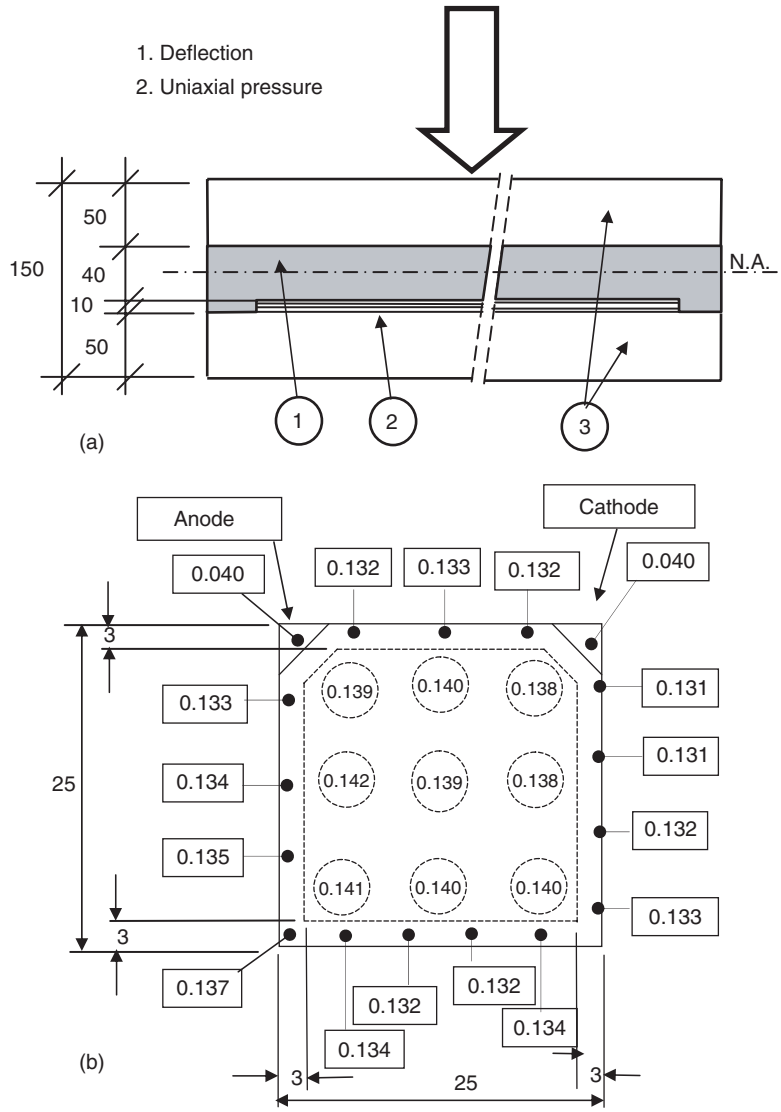

Figure 4. *(a) Cross section of thin-film energy cell (μm): 1. Surlyn sealant; 2. all-solid-state energy cell; 3. mica substrates; (b) thickness profile (mm): rectangles are thickness around edges, circles refer to the active component area.*

consists of similar top and bottom mica substrates of about 50 μm thickness each. The mica used for the substrates is muscovite, a phyllosilicate mineral of aluminum and potassium with chemical formula $KAl_2(AlSi_3O_{10})(F,OH)_2$ having a highly perfect basal cleavage that yields remarkably thin and highly elastic laminae. The energy cell mica substrates are held together by an all-around 40 μm polymer layer of Surlyn poly(ethylene-co-metahcrylic acid), EMAA (Dupont) sealant (Figure 4). In this present configuration and considering the packaging mass, the energy cells have a capacity of about 2 mAh/g and an energy density of about 8 Wh/kg.

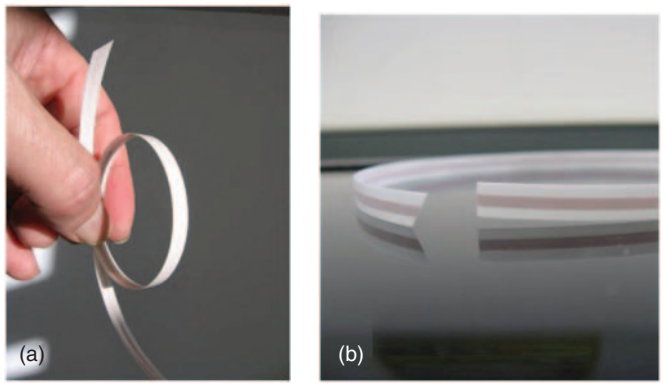

Figure 5. *(a) and (b): Flat flexible cable (FFC) 220 μm thick, single copper conductor, about 1.5 mm wide, insulated on both sides, rated at 100°C for continuous operation and 150°C for short periods.*

Two 12 K unidirectional carbon fiber prepregs were used: AS4/3502 Magnamite from Hexcel Corp. with a resin curing temperature of 177°C, and T700SC/RS-30G from YLA, Inc. with a lower resin curing temperature of 120°C and fiber areal weight (FAW) of 150 g/m^2. Both were assembled in $[0/90]_s$ configuration layups.

Nicomatic, Inc. provided polyester flat flexible cable (FFC) 220 μm thick, single copper conductor, about 1.5 mm wide, insulated on both sides, rated at 100°C for continuous operation and 150°C for short periods (Figure 5). This FFC was used to build the ingress/egress connections to and from the energy cell electrodes. The connections between the FFC and the energy cell electrodes themselves were done with high purity silver paint (SPI, Inc.) cured in a regular oven at standard atmospheric pressure and 65°C for 2–3 h.

The study was carried out in three consecutive stages: first, investigate the ability of the energy cells to withstand flexure, then their ability to withstand a minimum of about 550 kPa of uniaxial pressure required for autoclave curing, and finally, CFRP embedding. In all three stages, the charge/discharge performance of the energy cells was evaluated. The utmost attention and consideration was given to the preparation of the ingress/egress connections to and from the energy cell electrodes due to their fragility. The energy cell electrodes consist of a 100 nm thick copper layer (Cu, anode) and platinum (Pt, cathode) directly applied onto the mica (muscovite) bottom substrate (see Figures 2(b) and 6). These electrodes were found to be extremely fragile and easily peeled off from the substrate with just minimal stresses. Prior to embedding, the energy cells were pre-sealed, pre-encapsulated and pre-cured with either vinyl ester resin or polyurethane and cured at standard atmospheric pressure in a regular oven at 65°C for 8 h. The two polymers were chosen due to the compatibility of their functional groups with the chemical structure of the substrate.

Except in situations for which only mechanical properties were of interest, the energy cells were initially subjected to three initial consecutive charge/discharge cycles to establish a performance baseline for reference. The charging was done at a constant voltage of 4.2 VDC and a limiting current source of 1 mA using a Keithley SourceMeter 2400 under General Purpose Instrument Bus (GPIB) control of a Microsoft Development System (MDS) C program written specifically for this purpose by the author. The real time discrete current and voltage were measured at one-second intervals and logged to a text data file with cycle start/end times and time sequence for each data set. The energy cells

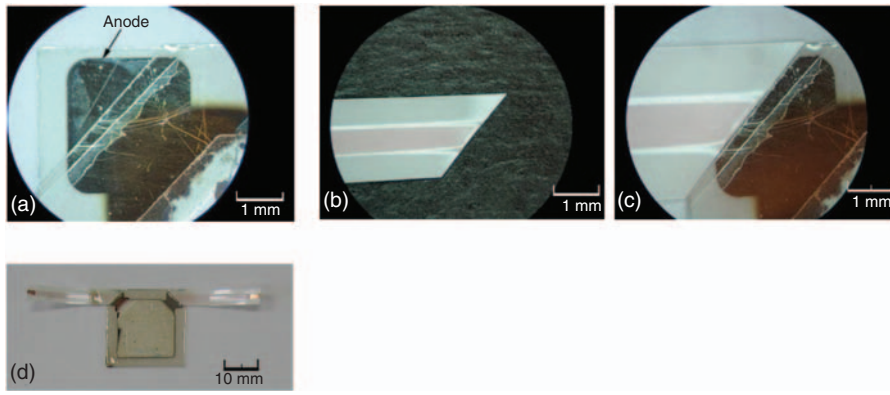

Figure 6. *(a) Energy cell Pt anode, about 2 mm on the side; (b) FFC cut at 45°; (c) FFC joined to anode, ready for sealing; (d) energy cell ready for embedding.*

were considered to be fully charged when the charge current fell below 50 μA while the voltage held constant at 4.2 VDC. Each charge cycle was immediately followed by a discharge at 1 mA constant sink current. Conversely, the energy cells were considered to be fully discharged when the voltage dropped to a value of 3.0 VDC. For the baseline performance profiles, the energy cell was charged and discharged without being subjected to any mechanical solicitations and at ambient conditions. The charge/discharge current of 1 mA used in this study corresponds to an average 2.5C discharge ratio (1 mA/0.4 mAh), which is more severe than the commonly used nominal discharge ratio of 1C found in the literature [12]. However, the former value is within the normal operating parameters for this type of energy cells, which can accept charge/discharge ratios higher than what are normally expected without suffering damage.

The discharge is used to define the energy cell capacity, C, in units of mAh. The discrete data acquired was taken to Matlab and integrated using the trapezoidal method to calculate the energy cell capacity, with the total charge/discharge adjusted for time accuracy. The energy cell capacity is defined as follows:

$$C = \int_0^{\tau} i \, dt, \tag{1}$$

where τ is the upper limit of integration corresponding to the time during charge at which the current $i(t) = 50\,\mu A$ is reached, or the time at which during discharge the voltage $v(t) = 3.0$ VDC is reached. The first three consecutive charge/discharge cycles were performed under no physical solicitations, and were used to establish the characteristic baseline profile of each energy cell.

The flexure capability of the energy cells was determined by applying a measured deflection in the middle of its span while measuring its ability to charge and discharge normally [8]. The flex ratio was calculated as the percentage between depth d and a constant span (Figure 7).

Uniform uniaxial pressure was measured at incremental steps using the fixture shown in Figure 8, with one complete charge and discharge cycle performed at every step while holding the uniaxial pressure constant [9].

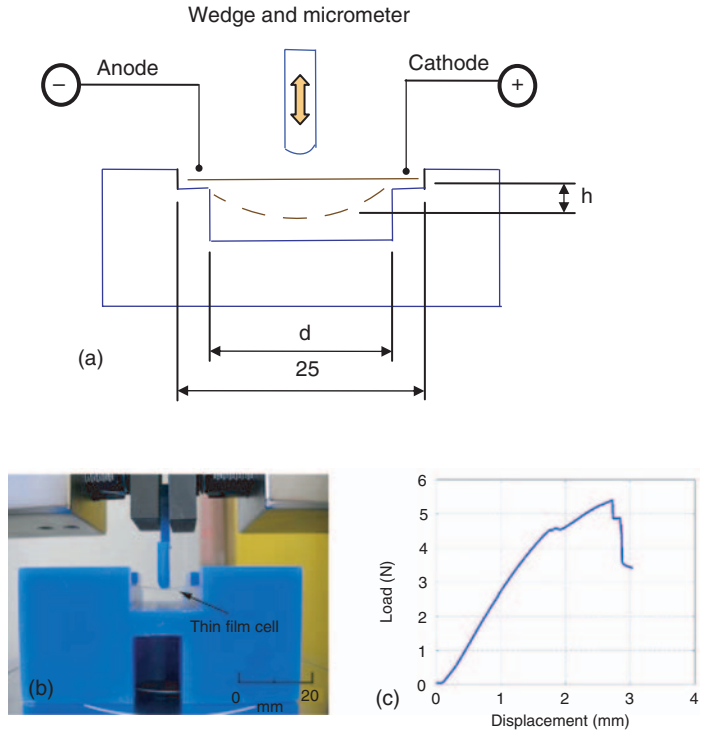

Figure 7. *(a) Flexure fixture diagram (mm); (b) rapid prototyped fixture installed on Instron machine; (c) load/displacement graph.*

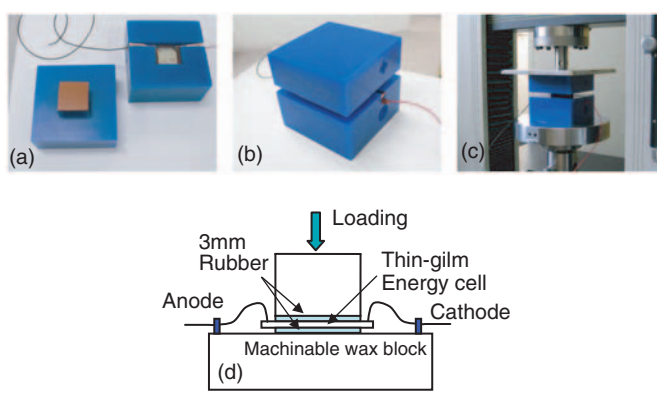

Figure 8. *(a) Uniaxial pressure fixture shown open, with energy cell inside; (b) pressure fixture closed; (c) mounted on the Instron machine; (d) schematic diagram.*

Thin film energy cells were embedded in the middle layer of $[0/90]_s$ as seen in the layup schematic of Figure 9(c). To determine their mechanical properties, tensile tests were performed on samples, as follows: (1) without embedded energy cells; (2) with embedded energy cells and without performing a charge/discharge cycle; (3) with embedded energy cells and charge/discharge cycle at 150 MPa uniaxial tensile stress increments [10].

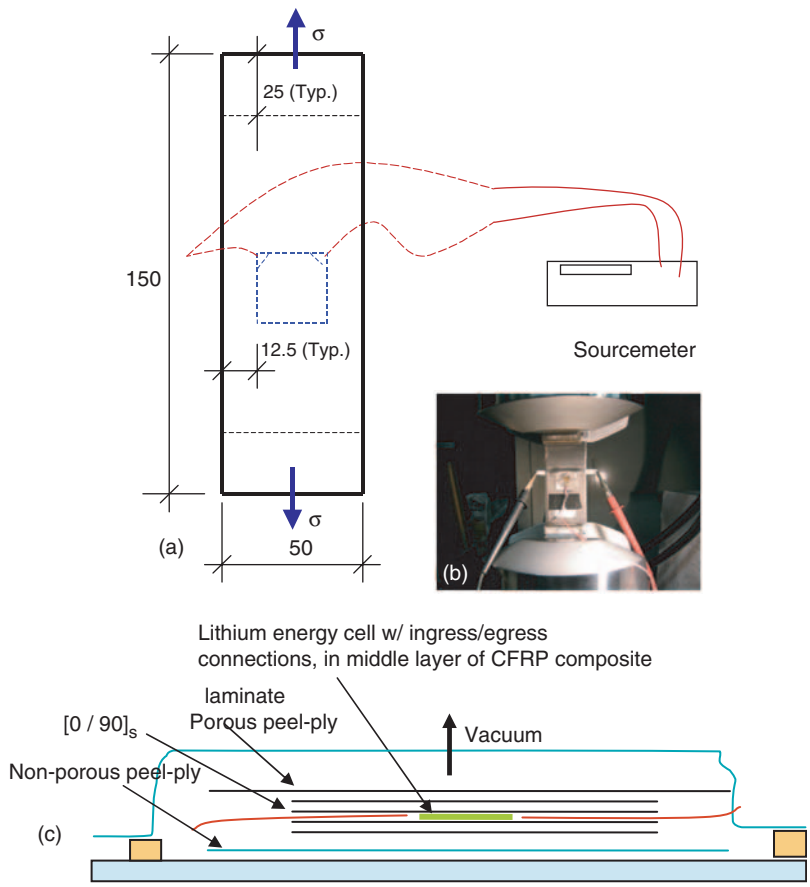

Figure 9. *Embedded energy cell setup; (a) schematic diagram (mm). The dimensions at each end are for the aluminum grip tabs; (b) specimen installed on an Instron 4483 for tensile testing and hooked up to a Keithley SourceMeter for charge/discharge capacity measurements; (c) lay-up schematic diagram.*

RESULTS AND DISCUSSION

The capability of thin-film energy cells to withstand flexural deformation was first investigated, albeit it was considered to be less of a critical factor to successfully embed the energy cells in CFRPs [8]. Figure 10 shows the typical results for one specimen undergoing flexural deflection in a pattern of increasing flex ratios alternating with un-deflected states. Up to about 1.3% deflection, no change in performance was observed. The difference between charge and discharge capacities indicates that only a small amount of energy is lost due to hysteresis. This energy dissipation is due to electrochemical losses inside the energy cell involving internal resistance and chemical changes, and it is transformed into heat and other losses. Figure 11 shows typical charge and discharge plots for the energy cells under deflection.

The capability of these all-solid-state energy cells to successfully endure a minimum pressure of 550 kPa required for autoclave fabrication was investigated [9]. This was a critical step to determine whether the thin-films could undergo autoclave fabrication and

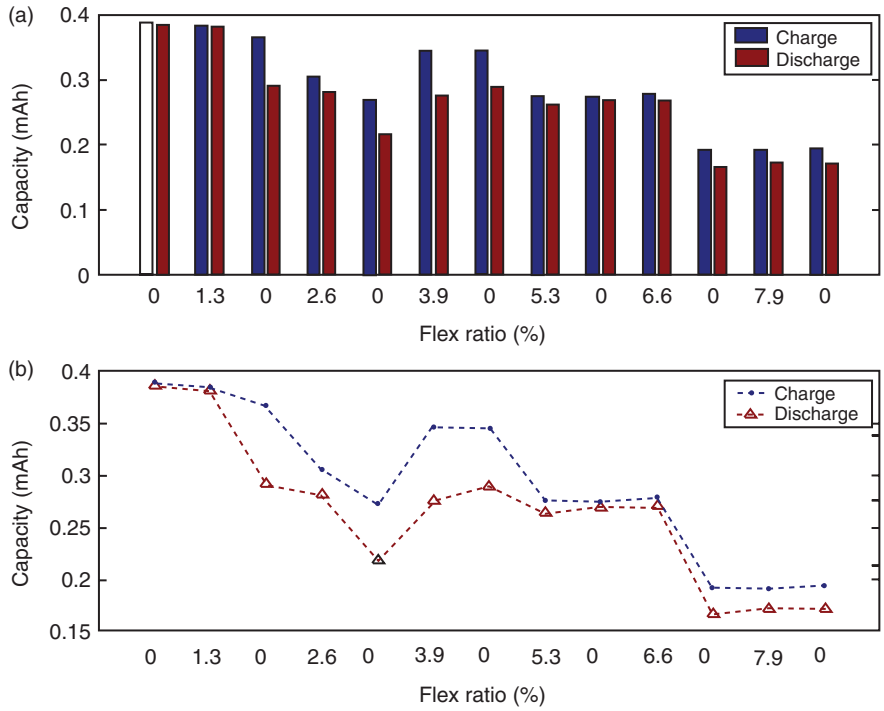

Figure 10. *Energy cell capacity under deflection: (a) left bar is charge, right bar is discharge; (b) line diagram shows more clearly the hysteresis between charge and discharge.*

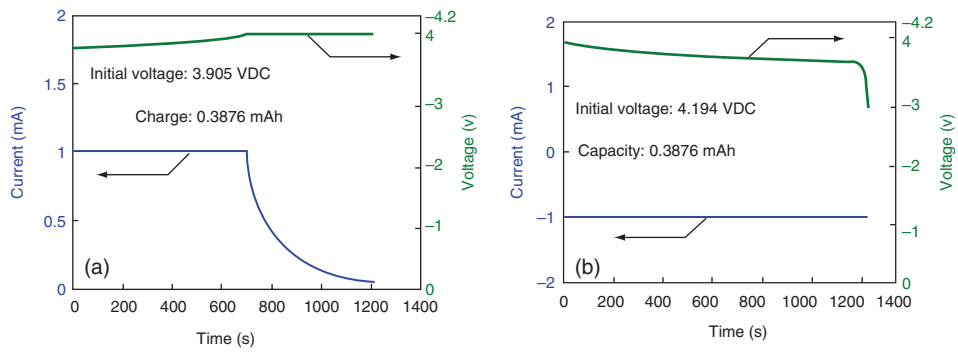

Figure 11. *Typical charge/discharge plots: (a) charge; (b) discharge.*

thus be good candidates for further embedding into CFRPs. A typical charge discharge plot for an energy cell under uniaxial pressure is shown in Figure 12. No significant loss of performance was observed up to about 2 MPa.

Uniaxial tensile test results for embedded configurations are summarized in Table 1 for AS4/3502 CFRPs and Table 2 for T700/RS30G. NE stands for non-embedded specimens and E stand for specimens embedded with energy cells. The embedded specimens in these two tables were not tested for charge/discharge while being subjected to uniaxial

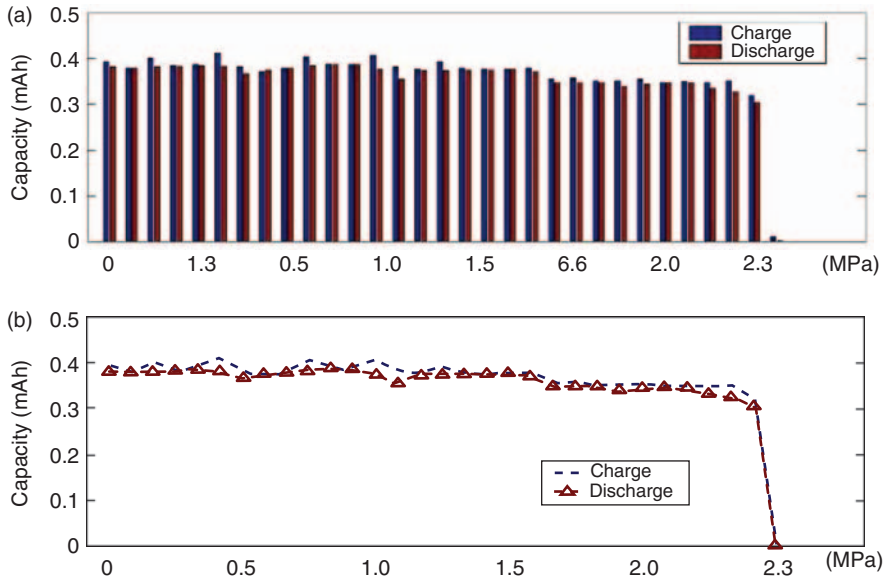

Figure 12. *Energy cell capacity under uniaxial pressure. Left bar is charge, right bar is discharge. The line diagram shows more clearly the hysteresis between charge and discharge.*

Table 1. AS4/3502 CFRP uniaxial tensile tests for embedded and non-embedded samples.

Lot No. – Sample No.	CFRP	Thick (mm)	Width (mm)	Gage (mm)	Modulus (GPa)	Strength (MPa)	Strain (%)
#1-1-NE	AS4/3502	0.64	51.5	61.84	34,160	803.4	2.652
#1-2-NE	AS4/3502	0.63	50.95	62.82	40,520	773.2	1.974
#1-3-E	AS4/3502	0.55	51.34	75.18	47,040	872.6	1.902
#1-4-E	AS4/ 3502	0.54	51.0	74.36	49,440	917.2	1.883

Table 2. T700/RS30G CFRP uniaxial tensile tests for embedded and non-embedded samples.

Lot No. – Sample No.	CFRP	Thick (mm)	Width (mm)	Gage (mm)	Modulus (GPa)	Strength (MPa)	Strain (%)
#1-1-NE	T700SC/RS-30G	0.62	51.5	54.53	44,740	1,315	3.1
#1-2-NE	T700SC/RS-30G	0.62	50.95	54.97	44,970	1,221	2.97
#2-1-NE	T700SC/RS-30G	0.63	51.34	53.76	45,770	1,327	3.195
#2-2-E	T700SC/RS-30G	0.60	51.0	54.16	49,190	1,396	3.094

tensile loading. They were investigated only for any significant changes in mechanical properties due to having embedded energy cells in the CFRP composite. As it can be seen, the presence of a thin-film embedded device did not substantially alter the mechanical characteristics of the CFRP composite structure. The yield strength increased slightly for the CFRP specimens with embedded energy cells, when compared with the control

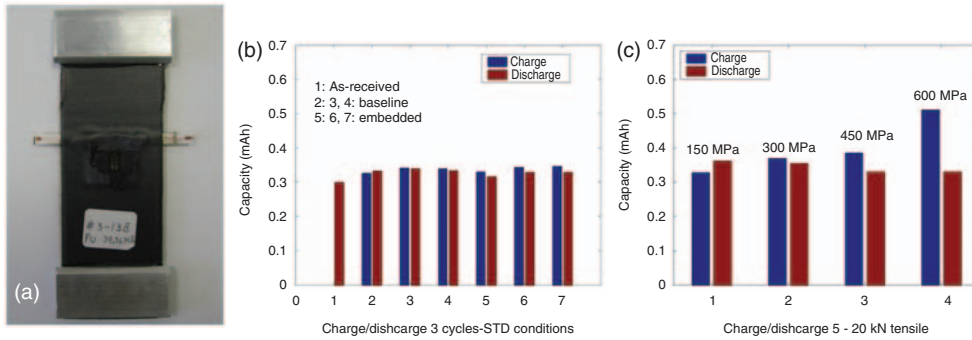

Figure 13. *Embedded energy cell capacity under uniaxial tensile loading. (a) CFRP coupon with embedded energy cell and ingress/egress connections; (b) as-received, baseline, and embedded performance; left bar is charge, right bar is discharge; (c) embedded performance with increasing uniaxial tensile loading.*

specimens with no embedded thin-film energy cells [10]. The CFRP rupture happened suddenly and without warning as revealed from the loading data obtained at 20 samples/s. The loading increased very close to linearly up to the last sample point in the data when the sample fractured. This was verified for all test coupons, embedded or non-embedded. Embedded energy cell capacity under uniaxial tensile is shown in Figure 13. Figure 13(a) shows a CFRP coupon with embedded energy cell and ingres/egress connections. Figure 13(b) shows as-received, baseline, and embedded performance, with the left bar representing charge, and the right bar discharge. Figure 13(c) shows embedded performance with increasing uniaxial tensile loading. At 600 MPa, the amount of energy required to charge the cell is significantly more than the energy obtained from discharge, indicating that damage in the energy cell occurred. However, the amount of energy that was discharged at this pressure was still significant when compared to baseline levels.

CONCLUSIONS

The construction of a laminated structural CFRP composite with energy storage capability was successfully demonstrated. The ability of the all-solid-state thin-film lithium energy cells to successfully withstand both flexure and pressure required for CFRP composite manufacturing in the autoclave was verified initially and was quantified. The charge/discharge rates of the embedded energy cells did not significantly deviate from standard charge/discharge baseline parameters obtained before embedding. Embedded energy cells did not show much deviation from the charge/discharge baseline performance when subjected to uniaxial tensile loadings up to 450 MPa. The maximum tensile load that was applied without degrading the performance of the embedded energy cell was found to be about 50% of the tensile strength of the CFRP.

ACKNOWLEDGMENTS

This work was carried out at the Multifunctional Composites Laboratory (MCL), University of California Los Angeles under the Air Force Office of Scientific

Research MURI Grant FA9550-05-1-0138 to the University of Washington, managed by Dr. B. Les Lee.

REFERENCES

1. Smith, D.L. (1995). *Thin Film Deposition: Principles and Practice*, McGraw-Hill, Inc., New York.
2. Raffaelle, R.P., Underwood, J., Scheiman, D., Cowen, J., Jenkins, P., Hepp, A.F., Harris, J. and Wilt, D.M. (2000). Integrated Solar Power Systems [Space Power Applications], In: *Photovoltaic Specialists Conference, Conference Record of the Twenty-Eighth IEEE 15–22*, pp. 1370–1373. doi 10.1109/PVSC.2000.916147.
3. Hucker, M.J. and Warsop. C. (2007). Integrating Bulk Piezoelectric Materials into MEMS for High Authority Actuators, *J. Micromech. Microeng.*, **17**: 1549–1557. doi:10.1088/0960-1317/17/8/018.
4. Mounier, E. and Eloya, J.-C. (2007). New Emerging MEMS Applications, In: *Proceedings of SPIE – The International Society for Optical Engineering*, Vol. 6462, Micromachining Technology for Micro-Optics and Nano-Optics V and Microfabrication Process Technology XII, p. 64620C.
5. Wise, K.D. (2007). Integrated Sensors, MEMS, and Microsystems: Reflections on a Fantastic Voyage, *Sensors and Actuators*, **A136**: 39–50.
6. Pines, D.J. and Bohorquez, F. (2006). Challenges Facing Future Micro-Air-Vehicle Development, *Journal of Aircraft*, **43**(2): 290–305.
7. Barrett, R. (2004). Adaptive Aerostructures: the First Decade of Flight on Uninhabited Aerial Vehicles, *Smart Structures and Materials*, Proceedings of SPIE, Vol. 5388.
8. Pereira, T., Scaffaro, R., Nieh, S., Arias, J., Guo, Z., and Hahn H.T. (2006). The Performance of Thin-Film Lithium Batteries under Deflection, *J. Micromech. Microeng.*, **16**: 2714–2721.
9. Pereira, T., Scaffaro, R., Nieh, S., Arias, J., Guo, Z. and Hahn, H.T. (2008). The Performance of All-Solid-State Thin-Film Lithium Energy Cells under Uniaxial Pressure, *Advan. Eng. Maters.*, **10**(4): 393–399. doi: 10.1002/adem.200700214.
10. Pereira, T., Guo, Z., Nieh, S., Arias, J. and Hahn, H.T. (2008). Embedding Thin-Film Lithium Energy Cells in Structural Composites, *Composites Science Technology*, **68**(7–8): 1935–1941. doi:10.1016/j.compscitech.2008.02.019.
11. Krasnov, V., Kai-Wei Nieh, and Su-Jen Ting (2003). Thin Film Battery and Method of Manufacture, Lithium-Ion U.S. Patent No. 6,632,563, http://www.uspto.gov/
12. Croce, F., Fiory, F.S., Persi, L. and Scrosati, B. (2001). A High-Rate, Long-Life, Lithium Nanocomposite Polymer Electrolyte Battery, *Electrochem. Solid-State Lett.*, **4**(8): A121–A123.